

Current-driven domain wall dynamics in ferrimagnetic Ni-doped Mn_4N films : very large domain wall velocities and reversal of motion direction across the magnetic compensation point

Sambit Ghosh,^{†,‡} Taro Komori,[‡] Ali Hallal,[†] Jose Peña Garcia,[¶] Toshiki Gushi,^{‡,†}
Taku Hirose,[‡] Haruka Mitarai,[‡] Hanako Okuno,[§] Jan Vogel,[¶] Mairbek
Chshiev,^{†,||} Jean-Philippe Attané,[†] Laurent Vila,^{*,†} Takashi Suemasu,[‡] and
Stefania Pizzini^{*,¶}

[†]*Univ. Grenoble Alpes, CEA, CNRS, Grenoble INP, IRIG-Spintec, 38054 Grenoble, France*

[‡]*Institute of Applied Physics, Graduate School of Pure and Applied Sciences, University of
Tsukuba, Tsukuba, Ibaraki 305-8573, Japan*

[¶]*Univ. Grenoble Alpes, CNRS, Institut Néel, 38042 Grenoble, France*

[§]*Univ. Grenoble Alpes, CEA, IRIG-MEM, 38000 Grenoble, France*

^{||}*Institut Universitaire de France, 75231, Paris, France*

E-mail: laurent.vila@cea.fr; stefania.pizzini@neel.cnrs.fr

Abstract

Spin-transfer torque (STT) and spin-orbit torque (SOT) are spintronic phenomena allowing magnetization manipulation using electrical currents. Beyond their fundamental interest, they allow developing new classes of magnetic memories and logic devices, in particular based on domain wall (DW) motion. In this work, we report the study of

STT driven DW motion in ferrimagnetic manganese nickel nitride ($\text{Mn}_{4-x}\text{Ni}_x\text{N}$) films, in which magnetization and angular momentum compensation can be obtained by the fine adjustment of the Ni content. Large domain wall velocities, approaching 3000 m/s, are measured for Ni compositions close to the angular momentum compensation point. The reversal of the DW motion direction, observed when the compensation composition is crossed, is related to the change of direction of the angular momentum with respect to that of the spin polarization. This is confirmed by the results of *ab initio* band structure calculations.

Introduction

Domain walls (DWs) separate magnetic domains present in ferromagnetic materials. Current-driven DW motion was predicted theoretically by Berger in 1978¹ and then extensively studied for its potential applications in domain wall racetrack memories², DW MRAM³, spin torque majority gate^{4,5} and other domain-wall-based logic devices⁶⁻⁹. The two mechanisms leading to DW motion driven by spin polarized currents are the spin-transfer torque (STT) and the spin orbit torque (SOT) associated to the spin Hall effect (SHE)¹⁰. While in the case of STT the charge current is spin polarized within the ferromagnetic layer by *sd* exchange interaction¹¹⁻¹³, in the case of SHE-SOT, the spin polarized current is generated by SHE in a neighbouring film (Pt, W, Ta ..), and then injected into the ferromagnetic layer¹⁴⁻¹⁷, resulting in both cases into a torque applied on the DWs.

Studies on systems in which domain walls are driven by STT are nowadays rare, mainly because there are practically no reports of efficient STT in thin films with perpendicular magnetization. In the last decade the interest of the spintronic community has focused on thin ferromagnetic films deposited on a heavy metal, where the interfacial Dzyaloshinskii-Moriya interaction (DMI) stabilizes chiral Néel walls that can be efficiently driven by SHE-SOT^{16,17}.

Recently, current-induced magnetization dynamics in ferrimagnets has become an active

field of research. In these materials, two magnetic sub-lattices are anti-ferromagnetically coupled, and the magnetization and angular momentum compensation of the two sublattices may be obtained by varying either the temperature or the composition of the material. Previous experiments on ferrimagnets¹⁸⁻²¹, mostly carried out on thin films deposited on a heavy metal, have evidenced new physical mechanisms taking place in the vicinity of these compensation points, leading to large SOT-driven DW velocities^{18,19}.

In the present work we report the study of ferrimagnetic Mn₄N thin films doped with Ni, in which magnetization and angular momentum compensation can be obtained by the fine adjustment of the Ni content. In these films, neither bulk nor interfacial DMI are present; domain walls have then a Bloch internal structure and are driven by STT. Our Kerr microscopy measurements show that due to the relatively large spin polarization of the conduction electrons and to the reduced angular momentum close to the compensation composition, domain walls can be driven by STT with an unprecedented efficiency. The reversal of the DW motion direction, observed when the compensation composition is crossed, is related to the change of direction of the angular momentum with respect to that of the spin polarization. This is confirmed by the results of *ab initio* band structure calculations.

Structural, magnetic and transport properties

Ferrimagnetic Mn₄N grows with a tetragonal anti-perovskite crystal structure (Fig. 1a), with two types of Mn atoms at the corner (site I) and at the face centred sites (site II). The two magnetic sublattices are anti-ferromagnetically coupled, with the net magnetization parallel to the Mn(I) moment. With a high Curie temperature of 745K²²⁻²⁵, a low magnetization (around 70-150 kA/m), and a relatively high uniaxial perpendicular anisotropy (0.1×10^6 MJ/m³)²⁶⁻³¹, this rare-earth free material is an interesting candidate for spintronic applications.

Using either pulsed-laser deposition²⁹, DC reactive sputtering²⁸ or molecular beam epi-

taxy^{27,30}, Mn₄N thin films can be grown on different substrates such as Si²⁶, SiC and GaN³², MgO²⁷⁻³¹, SrTiO₃ (STO)^{27,31,33} and (LaAlO₃)_{0.3}(Sr₂TaAlO₆)_{0.7} (LSAT)³⁴. Mn₄N films deposited on STO(001) were shown to exhibit smooth magnetic domains (at the mm scale), due to a reduced density of pinning sites³³, and record current-induced domain wall velocities driven by STT (900 m/s for J=1.3 TA/m²)³⁵.

In this paper, we focus on Ni-doped Mn₄N thin films epitaxially grown on STO(001) substrates³⁶. 10 nm and 30 nm thick Mn_{4-x}Ni_xN films, with nominal x varying between 0.1 and 0.25, were grown by molecular beam epitaxy on STO(001) substrates and capped with a 3 nm thick SiO₂ layer. Scanning transmission electron microscopy (STEM), reflection high-energy electron diffraction and X-ray diffraction measurements were performed to check their crystalline quality. The high resolution STEM micrograph of a 30 nm thick Mn_{3.75}Ni_{0.25}N film shown in Fig. 1b illustrates a highly ordered crystalline structure, with a negligible density of defects. The high-angle annular dark field scanning transmission electron microscopy (HAADF-STEM) image of the full stack and the elemental maps of Mn, O and Ni obtained by energy-dispersive X-ray spectroscopy (EDX), are shown in Fig. 1c-f. These data demonstrate that the distribution of the Ni atoms throughout the film has a good uniformity. On the other hand, while oxygen is mostly concentrated in the substrate and in the capping layer, a small region of the film, at the interface with the capping layer, appears to be oxidized. This layer has to be considered as a magnetically dead layer.

Our previous X-ray magnetic circular dichroism (XMCD) measurements³⁶ showed that Ni occupies preferentially the Mn(I) sites of Mn₄N. Since the moment carried by Ni atoms is anti-parallel to that of Mn(I), increasing the Ni atomic content allows reducing the overall magnetization. Beyond a critical Ni content, the net magnetization direction is thus expected to reverse with respect to the original one, i.e. to become anti-parallel to the Mn(I) magnetization. An analytical calculation of M_s using the magnetic moments of Mn(I), Mn(II) and Ni atoms extracted from neutron diffraction measurements^{22,25} predicts the magnetization compensation to occur for $x = 0.18$, corresponding to 3.6 at% of Ni. The presence of a mag-

netization compensation point around this Ni content was proved by XMCD measurements and confirmed by the sign reversal of the anomalous Hall angle for samples with Ni content on either side of it³⁷. The effect of the substitution of Mn(I) atoms with Ni atoms on the net magnetization is sketched in Fig. 1a: the net magnetization is parallel to the Mn(I) moment below the compensation point ($x = 0, 0.12$) and becomes parallel to the Mn(II) moment above it ($x = 0.25$).

The anomalous Hall effect (AHE) curves measured for $\text{Mn}_{4-x}\text{Ni}_x\text{N}$ films patterned into Hall crosses and Van der Pauw method on blanket layers are shown in Fig. 2a as a function of the Ni concentration ($x = 0, 0.15, 0.2$ and 0.25). The sharp magnetization switching observed for all the films reveals that they retain the large perpendicular magnetic anisotropy after patterning. A switch of the AHE angle from negative to positive is observed for Ni content between $x = 0.15$ and $x = 0.2$. This shows that the relative orientation of spin polarization and magnetic moment changes between these two values, confirming the previously obtained compensation composition for $x \approx 0.18$.

Fig. 2b shows the variation of the spontaneous magnetization M_s as a function of the Ni content, measured by vibrating sample magnetometry (VSM-SQUID) at room temperature. For each sample, the direction of the net magnetization is deduced from the sign of the AHE angle (as in Fig. 2a): positive/negative sign of M_s in the Fig. 2b indicates net magnetization parallel/anti-parallel to the Mn(I) magnetic moment. In agreement with previous results^{36,37}, M_s is observed to decrease with increasing Ni content and to change direction for x between 0.15 and 0.2. Note that for the nominal Ni content $x = 0.15$, a difference in the net magnetization direction is observed between the 10 nm and 30 nm thick films. This might be due to a small deviation from the targeted 3 at% of Ni content in the two films. For this reason, in Fig. 2b the shaded area indicates the deviation from the nominal Ni content x at the compensation point observed in this series of samples.

Domain wall dynamics

The domain wall dynamics in the $\text{Mn}_{4-x}\text{Ni}_x\text{N}$ films was studied at room temperature using polar magneto-optical Kerr effect (MOKE) microscopy, with differential imaging to enhance the magnetic contrast. The samples were patterned into 1 μm -wide strips using electron beam lithography and ion milling. The image of a complete device is shown in Fig. 3a. Fig. 3b shows differential MOKE images illustrating, with black and white contrasts, the displacements of the domain walls in opposite directions during the application of opposite current pulses. As expected, for a given current polarity, all the DWs move in the same direction.

Fig. 3c shows the DW velocities as a function of current density J , measured for samples with Ni content on both sides of the magnetization compensation composition, together with that of the undoped Mn_4N sample. For compositions below the magnetization compensation point (MCP), the DWs move in the direction of the electron flow and their mobility (dv/dJ) increases as the Ni concentration increases (*i.e.* as the net magnetization decreases). For compositions above the MCP, the DWs direction of motion reverses, and very large velocities in the direction of the the current flow, approaching 3000 m/s, are obtained for a Ni content around $x = 0.25$ ($M_S \approx -20$ kA/m) and current density $J = 1.2 \times 10^{12}$ A/m². Away from the compensation composition the DW mobility decreases and reaches values similar to those obtained for Mn_4N . The large mobilities obtained close to the magnetic compensation composition exceed the largest SOT-driven velocities measured in ferrimagnetic GdCo/Pt thin films, close to the angular momentum compensation at 250 K¹⁹.

In order to explain these results, let us compare them with the predictions of the collective coordinate $q - \phi$ model, expanded to a ferrimagnetic system consisting of two sub-lattices "1" and "2", using effective magnetic parameters^{38,39}.

In Mn_4N , the two magnetic sublattices "1" and "2" are composed of the same atomic species, Mn(I) and Mn(II), while in the $\text{Mn}_{4-x}\text{Ni}_x\text{N}$ films at most 5 at% of Mn(I) atoms are replaced by Ni atoms. In the absence of a precise measurement of the individual gyromagnetic

factors γ , and because of the small amount of Ni, we may then assume that $\gamma_1 = \gamma_2$. As a consequence, the magnetic and angular compensation points coincide. Furthermore, the strong anti-ferromagnetic coupling leads us also to consider that $\alpha_1 = \alpha_2$. In the asymptotic precessional regime i.e. well above the critical current density J_c ($\approx 2 \times 10^{10}$ A/m² for Mn₄N)³⁵, the DW velocity driven by STT reads^{38,39}:

$$\mathbf{v} = \frac{L_S + L_\alpha \beta}{L_S^2 + L_\alpha^2} L_S \mathbf{u} \quad (1)$$

where $L_S \mathbf{u} = PJh/(2e)\mathbf{e}_J$, $J\mathbf{e}_J$ is the current density, $P = P_1 - P_2$ is the effective spin polarization of the current, α is the Gilbert damping parameter, β characterizes the non-adiabatic contribution to the STT, $L_S = (M_1 - M_2)/\gamma$ is the angular momentum density and $L_\alpha = (\alpha/\gamma)(M_1 + M_2)$.

In Fig. 3d the experimental domain wall velocities obtained from Fig. 3c for $J = 1 \times 10^{12}$ A/m² are plotted versus $M_S = (M_1 - M_2) = \gamma L_S$. The best fit of the experimental data using Eq.1 is obtained for $P=0.65$, $\alpha=0.013$ and $\beta=0.002$.

The reversal of DW motion direction is expected to occur for $L_S = -\beta L_\alpha$, just below the angular compensation point. In the curve in Fig. 3c, the velocity vanishes just below the experimental magnetization compensation. This result appears to validate our assumption that $\gamma_1 = \gamma_2$, and therefore that the magnetization and angular momentum compensation coincide.

These results illustrate that the unprecedented large STT-driven DW velocities measured in Mn_{4-x}Ni_xN can be attributed to the increase of mobility when approaching the angular momentum compensation point (ACP), together to the relatively large net spin polarization of the conduction electrons. The reversal of the domain wall velocity predicted by the analytical model is based on the assumption that the sign of the spin polarization P does not change with the angular momentum density L_S . The DW motion reversal is therefore related to the change of relative orientation of the net spin polarization and the angular momentum, when the ACP is crossed.

In order to confirm the validity of this assumption, we have carried out *ab initio* band structure calculations.

***Ab initio* calculations**

First principles calculations were performed in the framework of density functional theory (DFT) using spin polarized relativistic Korringa-Kohn-Rostoker (SPR-KKR) and Vienna Ab Initio Simulation packages^{40–45,48–50}. The calculations for Mn₄N were based on the perovskite crystal structure ($Pm\bar{3}m$ space group) with lattice parameter of 3.74 Å and collinear magnetic configuration, as shown in Fig. 1a. The total magnetic moment along the [001] quantization axis was found to be 1 μ_B (Mn I: 3.3 μ_B , Mn II : -0.8 μ_B) in good agreement with previous calculations^{46,47}. Ni doping in Mn_{4-x}Ni_xN was taken into account using both the supercell approach and the coherent potential approximation (CPA) as implemented in SPR-KKR code^{48–50} (see Methods for details).

Fig. 4a shows that the calculated total magnetic moment decreases linearly with the Ni concentration and reverses direction with respect to the global quantization axis for $x=0.15$ using the SPR-KKR approach and for $x=0.17$ using the VASP approach, in good agreement with the experimental results. Fig.4b,c present the projected density of states (PDOS) calculated for the Mn(I) and Mn(II) sites of Mn₄N, while Fig. 4d,e,f show the s-PDOS of Ni substituted at site Mn(I), together with that of the Mn(I) and Mn(II) sites of Mn_{3.75}Ni_{0.25}N. For both samples the PDOS at the Fermi level (E_F) is about one order of magnitude larger for the Mn(II) site, with respect to that of the Mn(I) and the Ni sites. Moreover, it is larger for the majority (i.e. parallel to the global quantization axis) than the minority electrons. In summary, for compositions both below and above the ACP and MCP, the spin polarization of the conduction electrons is parallel to the (001) quantization axis and mostly due to the majority carriers in Mn(II) atoms. These results show that the sign of the polarization is the same below and above the ACP, confirming that our experimental results are in agreement

with the predictions of the $q - \phi$ model (Equation 1).

Conclusions

In conclusion, we have investigated $\text{Mn}_{4-x}\text{Ni}_x\text{N}$ ferrimagnetic thin films in which magnetization and angular momentum compensation can be obtained by a fine tuning of Ni doping. Current-driven domain wall velocity measurements were carried out for samples with various Ni content, having net magnetization on either sides of the compensation point. The domain wall velocities, driven by STT, are observed to increase for Ni compositions close to the ACP, that in these samples coincides with the MCP. Record domain wall velocities approaching 3000 m/s are observed for relatively low current densities ($J = 1.2 \times 10^{12}$ A/m²). These velocities, measured at room temperature and without the support of an in-plane magnetic field²¹, are of the same order of magnitude of those observed recently in ferrimagnetic thin films where DWs walls are driven by SHE-SOT^{19,21}.

The domain walls move in opposite directions for compositions on either sides of the ACP. This is related to the change of relative orientation of the net spin polarization and the angular momentum, when the ACP is crossed. Our results are in agreement with the predictions of the $q - \phi$ model, expanded to a ferrimagnetic system using effective parameters. *Ab initio* calculations validate the theoretical treatment by showing that the spin polarization of the conduction electrons is mainly due to majority carriers in the Mn(II) sub-lattice. The motion of DW parallel/antiparallel to the electron flow for composition below/above the compensation point is in agreement with this finding.

This work shows that although most of the recent efforts have focused on SOT-driven dynamics of DWs in thin films with DMI, STT appears to be also a very efficient way to drive DWs, provided that the film has a reduced magnetization (e.g. it is a ferrimagnet close to compensation points) and a relatively strong spin polarization. Our material, composed of abundant elements, and free of critical elements such as Co, rare earths and heavy metals,

is a promising candidate for sustainable spintronics applications.

Methods

Sample growth

The magnetic films were deposited on commercial 300 μm STO(100) substrates. The substrates were treated with HF and NH_4F solutions to smoothen the surface and were cleaned to remove any other impurities. 10 nm and 30 nm thick $\text{Mn}_{4-x}\text{Ni}_x\text{N}$ films were then epitaxially grown at 450° C with Mn and Ni atoms coming from the solid sources of high temperature Knudsen cells and using a radio-frequency nitrogen plasma source. The growth conditions were optimized at 1 nm/min with a N_2 gas flow of 0.9 cm^3/min with 4.1×10^{-3} Pa pressure in the chamber. To prevent further oxidation, the thin films were then capped in-situ with 3 nm of SiO_2 using a sputtering gun and an argon plasma source.

Ab initio calculations

The Vienna ab initio simulation package (VASP)^{40–42} was used for structure optimization, where the electron-core interactions are described by the projector augmented wave method for the potentials⁴³, and the exchange correlation energy is calculated within the generalized gradient approximation (GGA) of the Perdew-Burke Ernzerhof form^{44,45}. The cutoff energies for the plane wave basis set used to expand the Kohn-Sham orbitals were 500 eV for all calculations. Structural relaxations and total energy calculations were performed ensuring that the Hellmann-Feynman forces acting on ions were less than 10^{-2} N. Using a $44 \times 44 \times 44 \text{ \AA}^{-1}$ k-mesh the obtained bulk lattice constant of Mn_4N after full lattice relaxation was 3.74 \AA . Ni doping in $\text{Mn}_{4-x}\text{Ni}_x\text{N}$ were taken into account using the supercell approach, where we replaced an atom of Mn I by Ni in $1 \times 1 \times 4$ and $1 \times 1 \times 8$ unit cell to model $x = 0.25$ and $x = 0.125$, respectively. To verify the supercell approach we also calculated the effect of Ni doping in $\text{Mn}_{4-x}\text{Ni}_x\text{N}$ using the coherent potential approximation as implemented in

SPR-KKR code.

Domain wall velocity measurements

Polar magneto-optical Kerr microscopy was used to image the magnetic structure. Strong out-of-plane magnetic field pulses were used to nucleate reverse domains in the nucleation pads and to inject the domain walls into the nanowires. The domain walls were displaced by injecting both positive and negative 1 ns long current pulses. The shape of the pulses was captured and stored using an oscilloscope. The DW displacements from the different wires were averaged to obtain a precise estimation of the domain wall velocity. This was obtained by dividing averaged displacement by the averaged full width at half maximum (FWHM) of the pulse widths multiplied by the number of pulses.

Acknowledgements

We acknowledge Dr. Isogami from NIMS in Japan for the measurement of the damping factor. The devices were prepared in PTA platform from Grenoble, with partial support from the French RENATECH network. We acknowledge funding from IDEX-DOMINO project and JSPS KAKENHI (No. 19KK0104 and 19K21954). J.P.G. acknowledges the European Union's Horizon 2020 research and innovation program under Marie Skłodowska-Curie Grant Agreement No. 754303 and the support from the Laboratoire d'excellence LANEF in Grenoble (ANR-10-LABX-0051).

Author Information

Corresponding Authors

* E-mail: stefania.pizzini@neel.cnrs.fr

* E-mail: laurent.vila@cea.fr

Author Contributions

L.V., J.P.A., T.S. and S.P. managed the project and conceived the experiments. S.G., T.G., T.O., T.H., and H.M. prepared the samples. S.G. and T.G. realized the transport measurements. S.G. and T.G. performed the domain wall dynamics measurements with the guidance of S.P. H.O. made the TEM measurements. J.V. and S.G. performed the magnetization measurements. L.V., T. G. and S.G. patterned the samples by electron beam lithography. J.P.G. applied the analytical model to the experimental results. A. H. and M.C. made the ab initio calculations. S.P., J.P. A. and S.G. wrote the manuscript. All the authors discussed the results and commented on the manuscript.

References

- (1) Berger, L. Low-field magnetoresistance and domain drag in ferromagnets. *Journal of Applied Physics* **1978**, *49*, 2156–2161
- (2) Parkin, S.; Yang, S.-H. Memory on the racetrack. *Nature Nanotechnology* **2015**, *10*, 195–198
- (3) Brataas, A.; Kent, A. D.; Ohno, H. Current-induced torques in magnetic materials. *Nature Materials* **2012**, *11*, 372–381
- (4) Nikonov, D. E.; Bourianoff, G. I.; Ghani, T. Proposal of a Spin Torque Majority Gate Logic. *IEEE Electron Device Letters* **2011**, *32*, 1128–1130
- (5) Vaysset, A.; Manfrini, M.; Nikonov, D. E.; Manipatruni, S.; Young, I. A.; Pourtois, G.; Radu, I. P.; Thean, A. Toward error-free scaled spin torque majority gates. *AIP Advances* **2016**, *6*, 065304
- (6) Allwood, D. A. Submicrometer Ferromagnetic NOT Gate and Shift Register. *Science* **2002**, *296*, 2003–2006

- (7) Currivan, J. A.; Youngman Jang,; Mascaro, M. D.; Baldo, M. A.; Ross, C. A. Low Energy Magnetic Domain Wall Logic in Short, Narrow, Ferromagnetic Wires. *IEEE Magnetics Letters* **2012**, *3*, 3000104–3000104
- (8) Currivan-Incorvia, J. A.; Siddiqui, S.; Dutta, S.; Evarts, E. R.; Zhang, J.; Bono, D.; Ross, C. A.; Baldo, M. A. Logic circuit prototypes for three-terminal magnetic tunnel junctions with mobile domain walls. *Nature Communications* **2016**, *7*, 10275
- (9) Luo, Z.; Hrabec, A.; Dao, T. P.; Sala, G.; Finizio, S.; Feng, J.; Mayr, S.; Raabe, J.; Gambardella, P.; Heyderman, L. J. Current-driven magnetic domain-wall logic. *Nature* **2020**, *579*, 214–218
- (10) Slonczewski, J. Current-driven excitation of magnetic multilayers. *Journal of Magnetism and Magnetic Materials* **1996**, *159*, L1–L7
- (11) Freitas, P. P.; Berger, L. Observation of s - d exchange force between domain walls and electric current in very thin Permalloy films. *Journal of Applied Physics* **1985**, *57*, 1266–1269
- (12) Grollier, J.; Boulenc, P.; Cros, V.; Hamzić, A.; Vaurès, A.; Fert, A.; Faini, G. Switching a spin valve back and forth by current-induced domain wall motion. *Applied Physics Letters* **2003**, *83*, 509–511
- (13) Yamaguchi, A.; Ono, T.; Nasu, S.; Miyake, K.; Mibu, K.; Shinjo, T. Real-Space Observation of Current-Driven Domain Wall Motion in Submicron Magnetic Wires. *Physical Review Letters* **2004**, *92*, 077205
- (14) Khvalkovskiy, A. V.; Zvezdin, K. A.; Gorbunov, Y. V.; Cros, V.; Grollier, J.; Fert, A.; Zvezdin, A. K. High Domain Wall Velocities due to Spin Currents Perpendicular to the Plane. *Physical Review Letters* **2009**, *102*, 067206

- (15) Haazen, P. P. J.; Muré, E.; Franken, J. H.; Lavrijsen, R.; Swagten, H. J. M.; Koopmans, B. Domain wall depinning governed by the spin Hall effect. *Nature Materials* **2013**, *12*, 299–303
- (16) Emori, S.; Bauer, U.; Ahn, S.-M.; Martinez, E.; Beach, G. *Nat. Mater.* **2013**, *12*, 611
- (17) Ryu, K.-S.; Thomas, L.; Yang, S.-H.; Parkin, S. Chiral spin torque at magnetic domain walls. *Nature Nanotechnology* **2013**, *8*, 527
- (18) Kim, K.-J.; Kim, S. K.; Hirata, Y.; Oh, S.-H.; Tono, T.; Kim, D.-H.; Okuno, T.; Ham, W. S.; Kim, S.; Go, G.; Tserkovnyak, Y.; Tsukamoto, A.; Moriyama, T.; Lee, K.-J.; Ono, T. Fast domain wall motion in the vicinity of the angular momentum compensation temperature of ferrimagnets. *Nature Materials* **2017**, *16*, 1187
- (19) Caretta, L. et al. Fast current-driven domain walls and small skyrmions in a compensated ferrimagnet. *Nature Nanotechnology* **2018**, *13*, 1154–1160
- (20) Siddiqui, S. A.; Han, J.; Finley, J. T.; Ross, C. A.; Liu, L. Current-Induced Domain Wall Motion in a Compensated Ferrimagnet. *Physical Review Letters* **2018**, *121*, 057701
- (21) Caretta, L.; Oh, S.-H.; Fakhrul, T.; Lee, D.-K.; Lee, B. H.; Kim, S. K.; Ross, C. A.; Lee, K.-J.; Beach, G. S. D. Relativistic kinematics of a magnetic soliton. *Science* **2020**, *370*, 1438
- (22) Takei, W. J.; Shirane, G.; Frazer, B. C. Magnetic Structure of Mn_4N . *Physical Review* **1960**, *119*, 122–126
- (23) Takei, W. J.; Heikes, R. R.; Shirane, G. Magnetic Structure of Mn_4N -Type Compounds. *Physical Review* **1962**, *125*, 1893–1897
- (24) Mekata, M. Magnetic Study on Mn_4N and its Related Compounds. *Journal of the Physical Society of Japan* **1962**, *17*, 796–803

- (25) Fruchart, D.; Givord, D.; Convert, P.; l'Heritier, P.; Senateur, J. P. The non-collinear component in the magnetic structure of Mn_4N . *Journal of Physics F: Metal Physics* **1979**, *9*, 2431–2437
- (26) Ching, K. M.; Chang, W. D.; Chin, T. S.; Duh, J. G.; Ku, H. C. Anomalous perpendicular magnetoanisotropy in Mn_4N films on Si(100). *Journal of Applied Physics* **1994**, *76*, 6582–6584
- (27) Yasutomi, Y.; Ito, K.; Sanai, T.; Toko, K.; Suemasu, T. Perpendicular magnetic anisotropy of Mn_4N films on $\text{MgO}(001)$ and $\text{SrTiO}_3(001)$ substrates. *Journal of Applied Physics* **2014**, *115*, 17A935
- (28) Kabara, K.; Tsunoda, M. Perpendicular magnetic anisotropy of Mn_4N films fabricated by reactive sputtering method. *Journal of Applied Physics* **2015**, *117*, 17B512
- (29) Shen, X.; Chikamatsu, A.; Shigematsu, K.; Hirose, Y.; Fukumura, T.; Hasegawa, T. Metallic transport and large anomalous Hall effect at room temperature in ferrimagnetic Mn_4N epitaxial thin film. *Applied Physics Letters* **2014**, *105*, 072410
- (30) Meng, M.; Wu, S. X.; Ren, L. Z.; Zhou, W. Q.; Wang, Y. J.; Wang, G. L.; Li, S. W. Extrinsic anomalous Hall effect in epitaxial Mn_4N films. *Applied Physics Letters* **2015**, *106*, 032407
- (31) Ito, K.; Yasutomi, Y.; Kabara, K.; Gushi, T.; Higashikozono, S.; Toko, K.; Tsunoda, M.; Suemasu, T. Perpendicular magnetic anisotropy in $\text{Co}_x\text{Mn}_{4-x}\text{N}$ ($x = 0$ and 0.2) epitaxial films and possibility of tetragonal Mn_4N phase. *AIP Advances* **2016**, *6*, 056201
- (32) Dhar, S.; Brandt, O.; Ploog, K. H. Ferrimagnetic $\text{Mn}_4\text{N}(111)$ layers grown on 6H-SiC(0001) and GaN(0001) by reactive molecular-beam epitaxy. *Applied Physics Letters* **2005**, *86*, 112504

- (33) Gushi, T.; Vila, L.; Fruchart, O.; Marty, A.; Pizzini, S.; Vogel, J.; Takata, F.; Anzai, A.; Toko, K.; Suemasu, T.; Attané, J.-P. Millimeter-sized magnetic domains in perpendicularly magnetized ferrimagnetic Mn_4N thin films grown on SrTiO_3 . *Japanese Journal of Applied Physics* **2018**, *57*, 120310
- (34) Hirose, T.; Komori, T.; Gushi, T.; Toko, K.; Suemasu, T. Perpendicular magnetic anisotropy in ferrimagnetic Mn_4N films grown on $(\text{LaAlO}_3)_{0.3}(\text{Sr}_2\text{TaAlO}_6)_{0.7}(0\ 0\ 1)$ substrates by molecular beam epitaxy. *Journal of Crystal Growth* **2020**, *535*, 125566
- (35) Gushi, T.; Jovicević Klug, M.; Peña Garcia, J.; Ghosh, S.; Attané, J.-P.; Okuno, H.; Fruchart, O.; Vogel, J.; Suemasu, T.; Pizzini, S.; Vila, L. Large Current Driven Domain Wall Mobility and Gate Tuning of Coercivity in Ferrimagnetic Mn_4N Thin Films. *Nano Letters* **2019**, *19*, 8716–8723
- (36) Komori, T.; Hirose, T.; Gushi, T.; Toko, K.; Hanashima, T.; Vila, L.; Attané, J.-P.; Amemiya, K.; Suemasu, T. Magnetic reversal in rare-earth free $\text{Mn}_{4-x}\text{Ni}_x\text{N}$ epitaxial films below and above Ni composition needed for magnetic compensation around room temperature. *Journal of Applied Physics* **2020**, *127*, 043903
- (37) Komori, T.; Gushi, T.; Anzai, A.; Vila, L.; Attané, J.-P.; Pizzini, S.; Vogel, J.; Isogami, S.; Toko, K.; Suemasu, T. Magnetic and magneto-transport properties of Mn_4N thin films by Ni substitution and their possibility of magnetic compensation. *Journal of Applied Physics* **2019**, *125*, 213902
- (38) Okuno, T.; Kim, D.; Oh, S. et. al. Spin-transfer torques for domain wall motion in antiferromagnetically coupled ferrimagnets. *Nat. Electron.* **2019**, *2*, 389
- (39) Haltz, E.; Krishnia, S.; Berges, L.; Mougín, A.; Sampaio, J. Domain wall dynamics in antiferromagnetically coupled double-lattice systems. *Phys. Rev. B* **2021**, *103*, 014444
- (40) Kresse, G.; Hafner, J. *Ab initio* molecular dynamics for liquid metals. *Physical Review B* **1993**, *47*, 558–561

- (41) Kresse, G.; Furthmüller, J. Efficiency of ab-initio total energy calculations for metals and semiconductors using a plane-wave basis set. *Computational Materials Science* **1996**, *6*, 15–50
- (42) Kresse, G.; Furthmüller, J. Efficient iterative schemes for *ab initio* total-energy calculations using a plane-wave basis set. *Physical Review B* **1996**, *54*, 11169–11186
- (43) Blöchl, P. E. Projector augmented-wave method. *Physical Review B* **1994**, *50*, 17953–17979
- (44) Perdew, J. P.; Burke, K.; Ernzerhof, M. Generalized Gradient Approximation Made Simple. *Physical Review Letters* **1996**, *77*, 3865–3868
- (45) Kresse, G.; Joubert, D. From ultrasoft pseudopotentials to the projector augmented-wave method. *Physical Review B* **1999**, *59*, 1758–1775
- (46) Meinert, M. Exchange interactions and Curie temperatures of the tetrametal nitrides Cr₄N, Mn₄N, Fe₄N, Co₄N, and Ni₄N. *Journal of Physics: Condensed Matter* **2016**, *28*, 056006
- (47) Isogami, S.; Masuda, K.; Miura, Y. Contributions of magnetic structure and nitrogen to perpendicular magnetocrystalline anisotropy in antiperovskite ϵ -Mn₄N. *Physical Review Materials* **2020**, *4*, 014406
- (48) Ebert, H.; Ködderitzsch, D.; Minár, J. Calculating condensed matter properties using the KKR-Green's function method - recent developments and applications. *Reports on Progress in Physics* **2011**, *74*, 096501
- (49) Ebert, H.; Braun, J.; Ködderitzsch, D.; Mankovsky, S. Fully relativistic multiple scattering calculations for general potentials. *Physical Review B* **2016**, *93*, 075145
- (50) Ebert, H.; Munich SPR-KKR band structure program package. <http://olymp.cup.uni-muenchen.de/ak/ebert/SPRKKR>, version 6.3, 2012 (accessed Sept. 7, 2018)

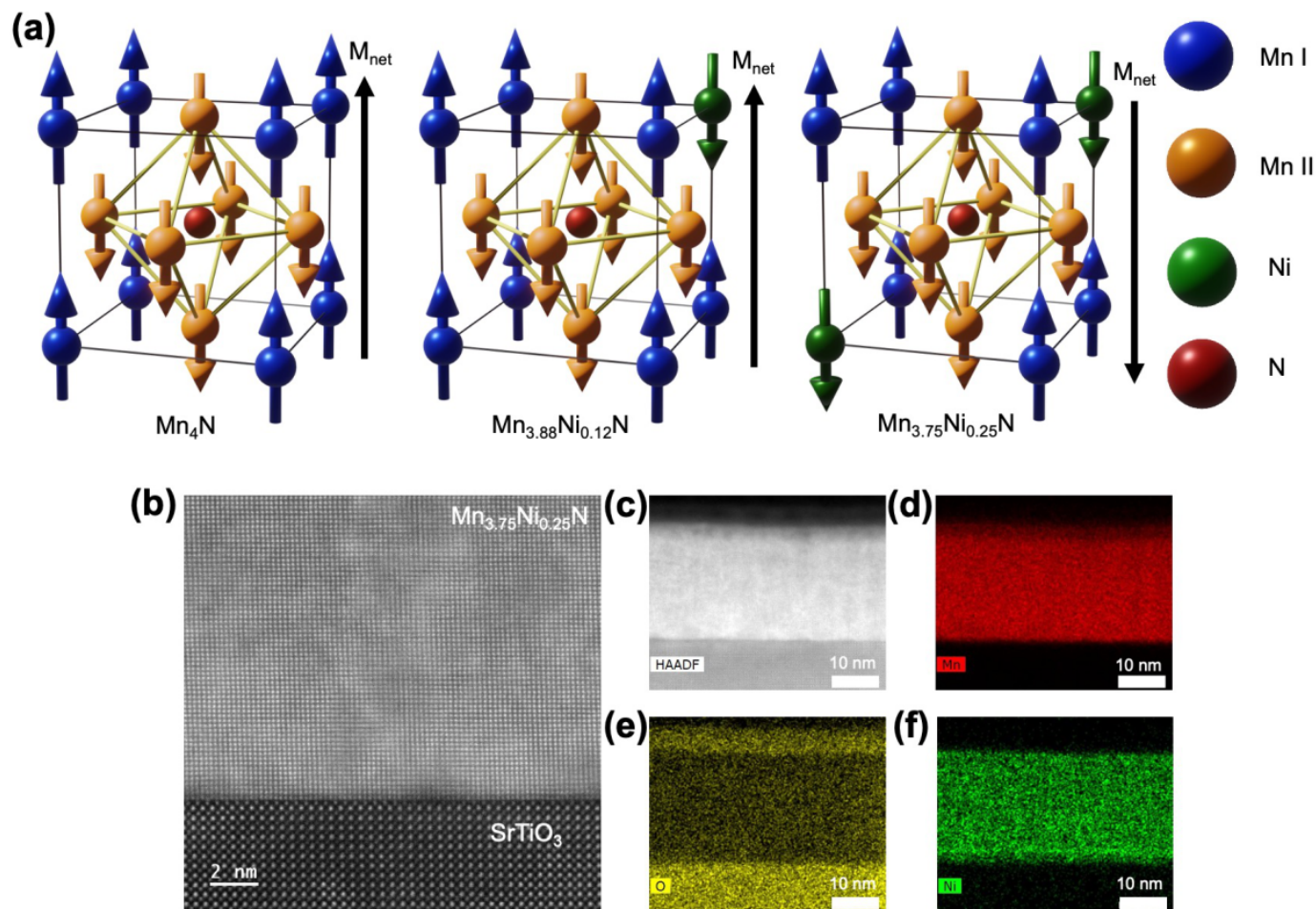


Fig. 1: (a) Schematics of the anti-perovskite crystal structure of Mn_4N (left), showing the substitution of the Mn(I) site atoms (in blue) with Ni atoms, to model $Mn_{1-x}Ni_xN$ (middle and right). Mn(II) atoms are shown in orange, Ni atoms in green and nitrogen atoms in red. Mn(I) magnetic moments are parallel to the [001] quantization axis. The net magnetization decreases when increasing the Ni concentration, and after crossing the magnetic compensation point the direction of the net magnetic moment is reversed. (b) High resolution STEM image of a 30 nm $Mn_{3.75}Ni_{0.25}N$ thin film deposited onto a STO substrate. (c) HAADFSTEM image of the full thin film with the capping layer of 3 nm SiO_2 and associated EDX elemental map of Mn (d), O (e) and Ni (f).

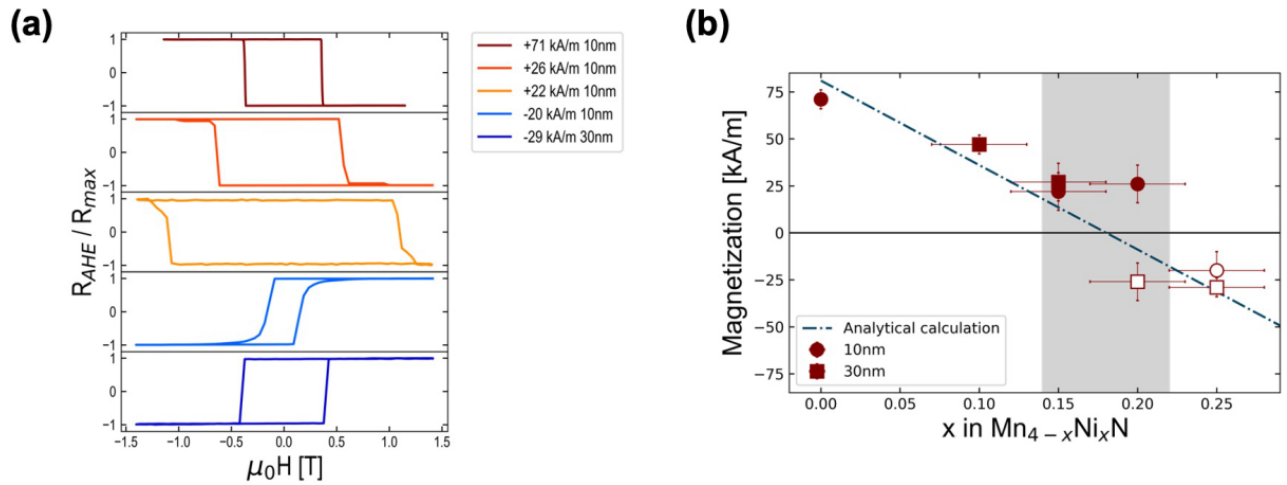


Fig. 2: (a) Anomalous Hall effect curves measured for thin films with different Ni concentrations ($x=0$ (10 nm), 0.15(10 nm), 0.2(10 nm), 0.25(10 nm) and 0.25(30 nm)). The sign of the Hall angle changes from negative to positive when crossing the magnetic compensation point between $x=0.15$ and $x=0.25$, indicating the change of direction of the net magnetization. The corresponding net magnetization values measured by VSM-SQUID are reported in the caption. (b) Spontaneous magnetization versus nominal Ni concentration x , measured for the $Mn_{4-x}Ni_xN$ thin films by VSM-SQUID. The sign of the net magnetization is obtained from the sign of the AHE angle. The shaded area indicates the spread of the observed deviation of the Ni content x at the compensation point, with respect to the nominal value. The dotted line shows the magnetization obtained analytically.

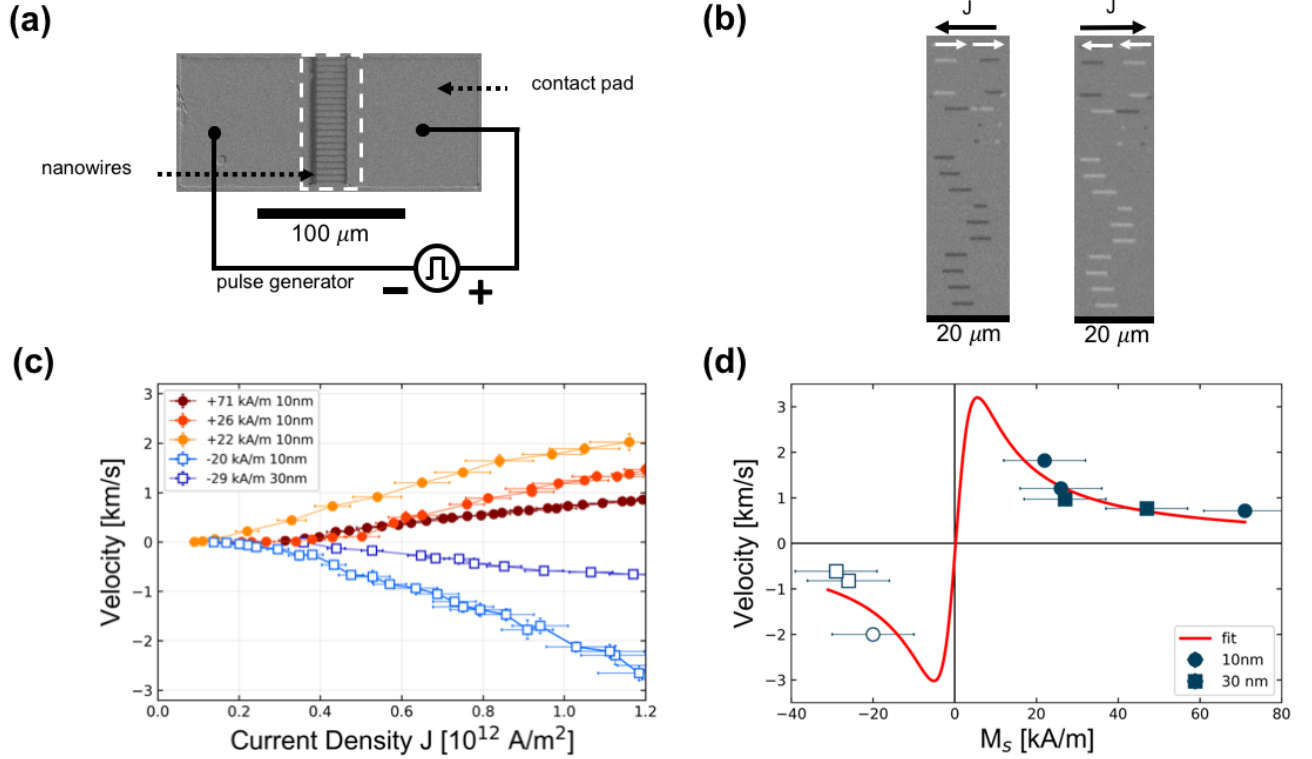


Fig. 3: (a) Sketch of the devices fabricated for the measurement of domain wall dynamics, showing twenty parallel nanowires where DWs are driven by polarized current pulses, together with the contact pads from which the DWs are injected. (b) Differential polar MOKE images, showing the displacement of domain walls during the application of a negative (left) and positive (right) current pulses. The white arrows indicate the DW displacement. In this device with composition below the compensation point, the DWs move in the direction of the electron flow. (c) Domain wall speed versus current density for $\text{Mn}_{4-x}\text{Ni}_x\text{N}$ films with different Ni concentration on either sides of the compensation point. $M_S=71$ kA/m corresponds to Mn_4N ($x=0$). The filled/empty symbols show the velocity below/above the compensation point: the DW direction of motion changes sign when crossing the compensation point. (d) The domain wall velocity versus net magnetization M_S , measured for $J=1 \times 10^{12}$ A/m² (black squares) is compared with the best fit obtained using the $q - \phi$ model (Eq. 1) (red line).

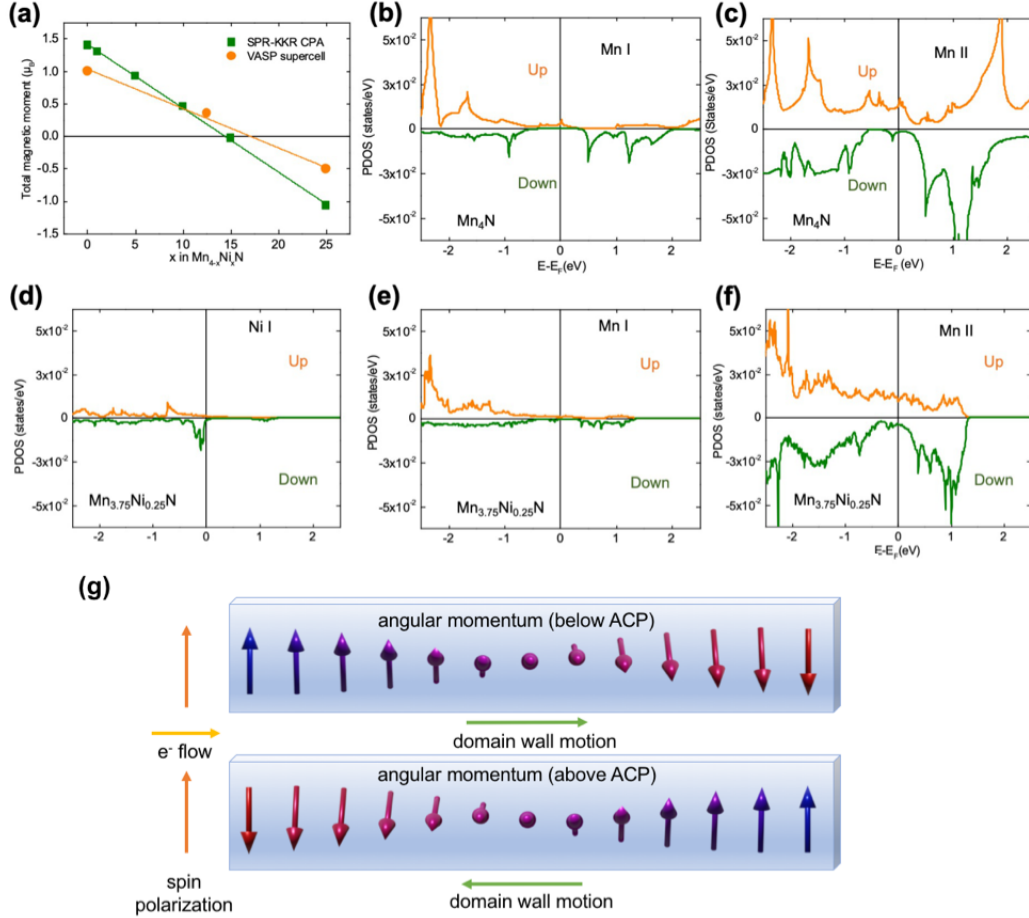


Fig. 4: (a) Ab initio calculation of magnetic moment versus Ni concentration showing a change in the net magnetization direction around $x=0.15$. (b) & (c) s-orbital PDOS of sites Mn(I) and Mn(II) of Mn_4N . The polarization direction at the Fermi level is "up" for both atoms while a much larger PDOS, determining the conduction electron carriers, is obtained for the Mn(II) site. (d),(e) & (f) s-orbital PDOS of Ni, Mn(I) and Mn(II) in $Mn_{3.75}Ni_{0.25}N$. The polarization direction at the Fermi level remains "up" for all the atoms. (g) Sketch of a Bloch domain wall with the individual net magnetic moments, for a sample below/above the angular momentum compensation point (top/bottom). The orange arrows indicates the direction of the spin polarization, that stays the same below and above the ACP. The yellow line indicates the direction of the electron flow. Since the spin polarization direction is the same, while the net angular momentum changes direction, the spin-transfer torque drives the DW in opposite directions below and above the ACP.

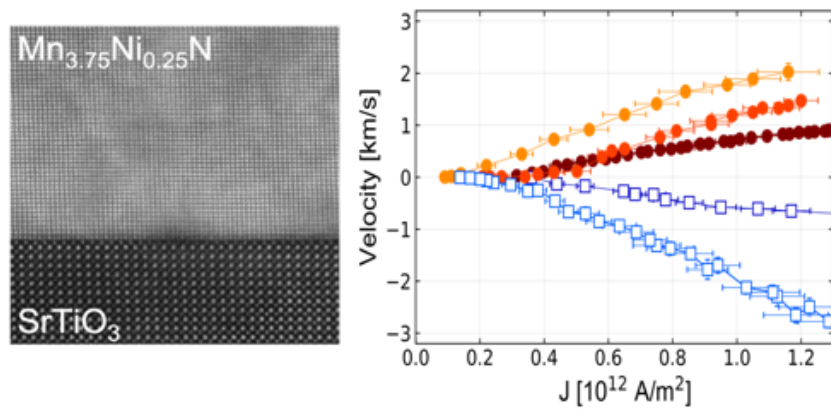


Fig. 5: Figure TOC